

Validation Cases for Aeolus ASP

Technical Report IR-17-01

Uwe Schuster
October 26, 2017

Contents

1	Introduction	3
2	Methodology	3
3	Results	5
3.1	Pressure Distribution	5
3.1.1	Straight Wing	5
3.1.2	Swept Wing	5
3.1.3	Boxwing	9
3.2	Induced drag	12
3.2.1	Comparison with CFD	12
3.2.2	Robustness in an optimization	12
4	Conclusions	15

Revisions

Revision	Date	Description
-	26 Oct 2017	Initial version

Symbols

Symbol	Description	Unit
α_{wt_i}	Twist angle of a certain wing section i	[-]
α_∞	Nominal angle of attack	[-]
b	Wing span	[m]
β	Reference area correction factor for non-planar wings	[-]
C_{di}	Induced drag coefficient	[-]
C_{dvisc}	Viscous drag coefficient	[-]
C_l	Lift coefficient	[-]
c_p	Local pressure coefficient	[-]
E	Lift-to-Drag ratio	[-]
F_{di}	Induced drag	[N]
F_l	Lift	[N]
h	Wing height (non-planar wigs)	[-]
Λ_P	Average panel aspect ratio	[-]
$\#\mathcal{P}_{ws}$	Number of panels per wing strip	[-]

1 Introduction

Aeolus ASP (Aero Sketch Pad) is particularly designed for fast, accurate, and robust aerodynamic analysis of any given wing. Therefore, a three-dimensional panel method kernel was developed, which employs various innovative improvements. This report is intended to validate this aerodynamic kernel in Aeolus ASP by means of comparison with wind tunnel tests and CFD results.

2 Methodology

The validation concerns

- wing surface pressure distribution
- induced drag

as these results govern all other aerodynamic properties. Therefore, three different reference wing configurations will be investigated. They are outlined in Figure 2.1.

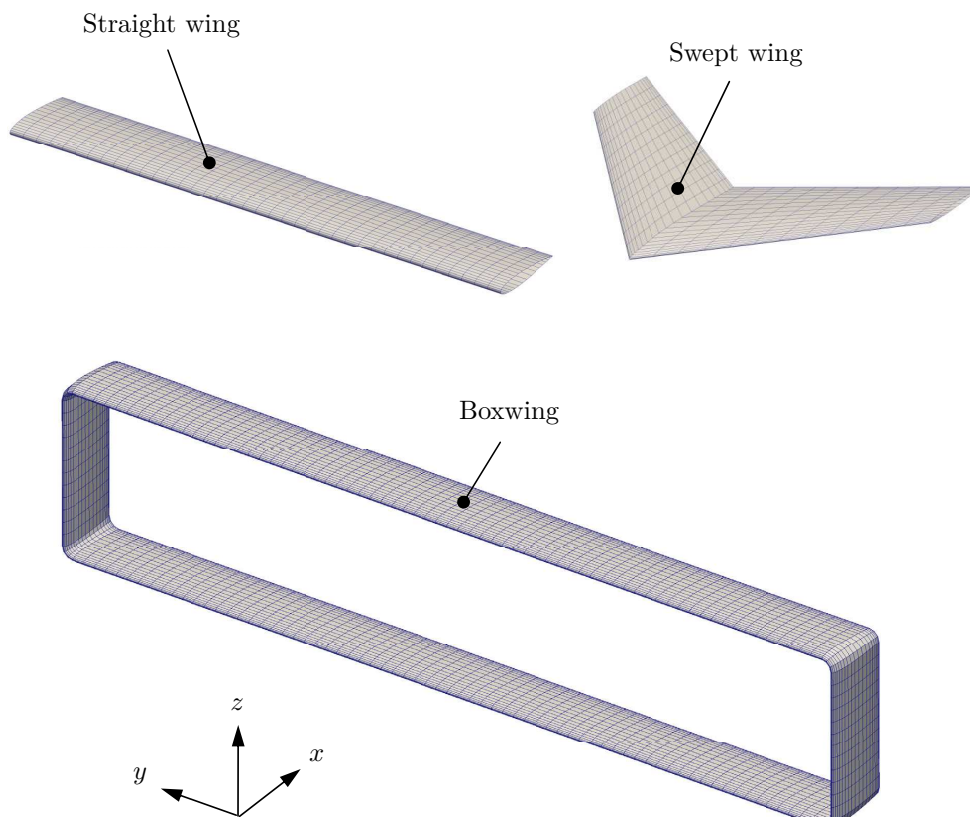


Figure 2.1: Overview of investigated wing configurations

The straight wing and the swept wing have been tested in the wind tunnel [1, 2], and the Boxwing was analysed by means of CFD [3]. More information can be found in Table 2.1.

Note, that these reference cases fulfill the three major requirements which allow comparison with potential theory results:

- Attached flow
- Compressibility effects negligible ($Ma \leq 0.3$)
- Viscosity effects negligible (high Re)

Table 2.1: Overview of wing parameters and available reference results

	Straight wing	Swept wing	Boxwing
Reference	Wind tunnel [1]	Wind tunnel [2]	CFD [3]
Airfoil	NACA 0015	NACA 64A010	NACA 0012
Aspect ratio Λ	6.6	3.0	6
Taper ratio λ	1.0	0.5	1
Sweep $\phi_{25\%}$	0°	45°	0°
Twist α_{wt}	0°	0°	0°
Re	$2.5 \cdot 10^6$	$18 \cdot 10^6$	-
Ma	0.3	0.25	-
α_∞	8°	8°	5.406°
C_l	-	-	0.5
C_{di}	-	-	$9.218e-3$
$C_l(y)$ -distribution	✓	✓	✓
$c_p(x)$ -distribution	✓	✓	-

The quality of the results obtained with Aeolus ASP depends on the panel mesh quality. A more dense mesh (i.e. more panels) typically yields more accurate results, however, computation time increases. It is therefore interesting to find a suitable balance, that is a "standard" resolution, which can be used for most cases. The resolution is mainly governed by two parameters:

- Number of panels per wing strip $\#\mathcal{P}_{ws}$
- Average panel aspect ratio Λ_P

Each wing will be investigated with two different resolutions, which are defined in Table 2.2. They correspond to a proposed standard resolution, and a very fine resolution, respectively. The intention is to show, that the standard resolution is sufficient for typical problems.

Table 2.2: Investigated panel resolutions in Aeolus ASP

Resolution	$\#\mathcal{P}_{ws}$	Λ_P
Standard (Std)	40	0.3
Fine	100	0.3

3 Results

3.1 Pressure Distribution

3.1.1 Straight Wing

Figure 3.1 shows the discretisation of the wing surface using the standard resolution, and the associated pressure distribution. Due to symmetry, the wind tunnel experiment [1] and the

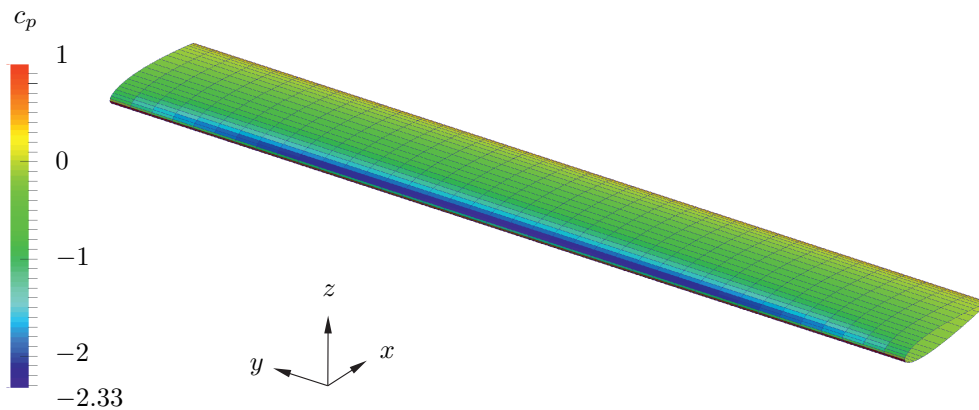


Figure 3.1: Aeolus ASP computed pressure distribution on the straight wing (std resolution)

Aeolus ASP model consist of the half-wing only. In the experiment, the surface pressure has been measured at different spanwise stations. In order to account for wind tunnel effects a correction has been applied as proposed in [1, p.15]. Figure 3.2 compares the resulting pressure distribution at selected spanwise stations to the Aeolus ASP results. Due to the large number of panels in the fine resolution, the results are plotted as a line rather than points. There is a good agreement between experiment and simulation. Errors are in the order of magnitude of typical systematic errors associated with wind tunnel experiments.

The station-wise pressures can be integrated to the spanwise lift distribution, which is shown in Fig. 3.3. Again, the comparison confirms good agreement. The fine resolution does not significantly improve the accuracy. Therefore, it can be noted, that the standard resolution is sufficient for this test case.

3.1.2 Swept Wing

With regard to the swept wing, the resulting pressure distribution, shown in Fig. 3.4, can also be compared to a wind tunnel experiment [2]. Figures 3.5 and 3.6 demonstrate the good agreement at three different spanwise stations.

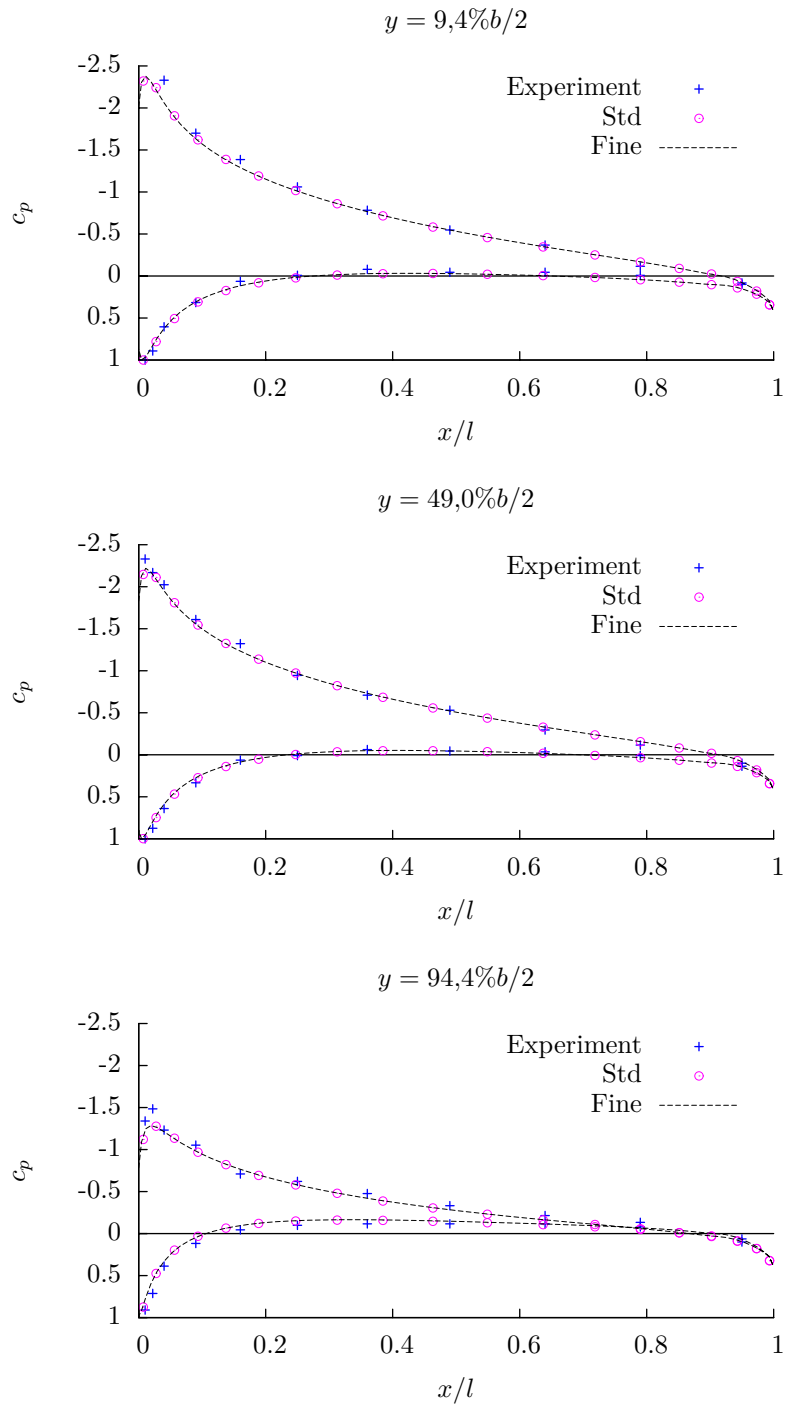


Figure 3.2: Comparison of the pressure distribution on the straight wing

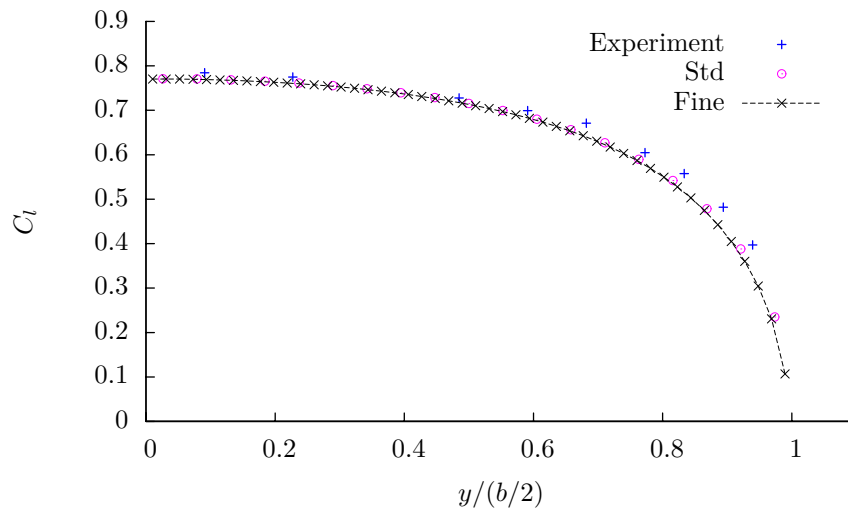


Figure 3.3: Comparison of the lift distribution on the straight wing

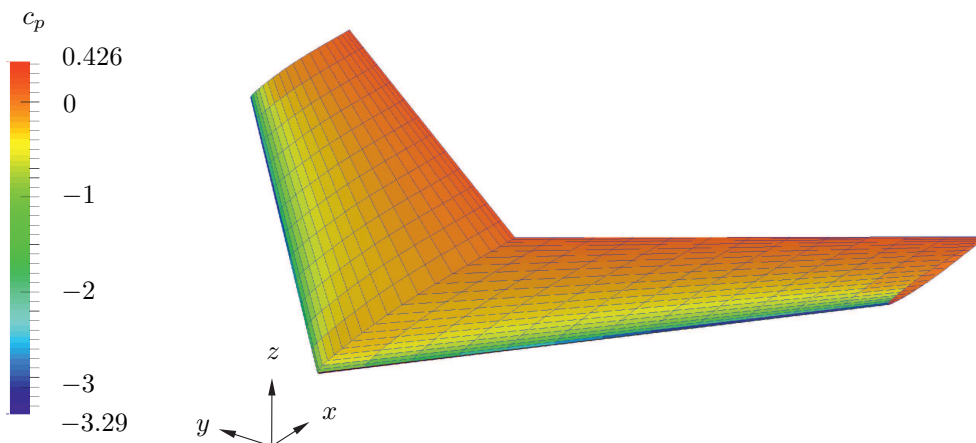


Figure 3.4: Aeolus ASP computed pressure distribution on the swept wing (std resolution)

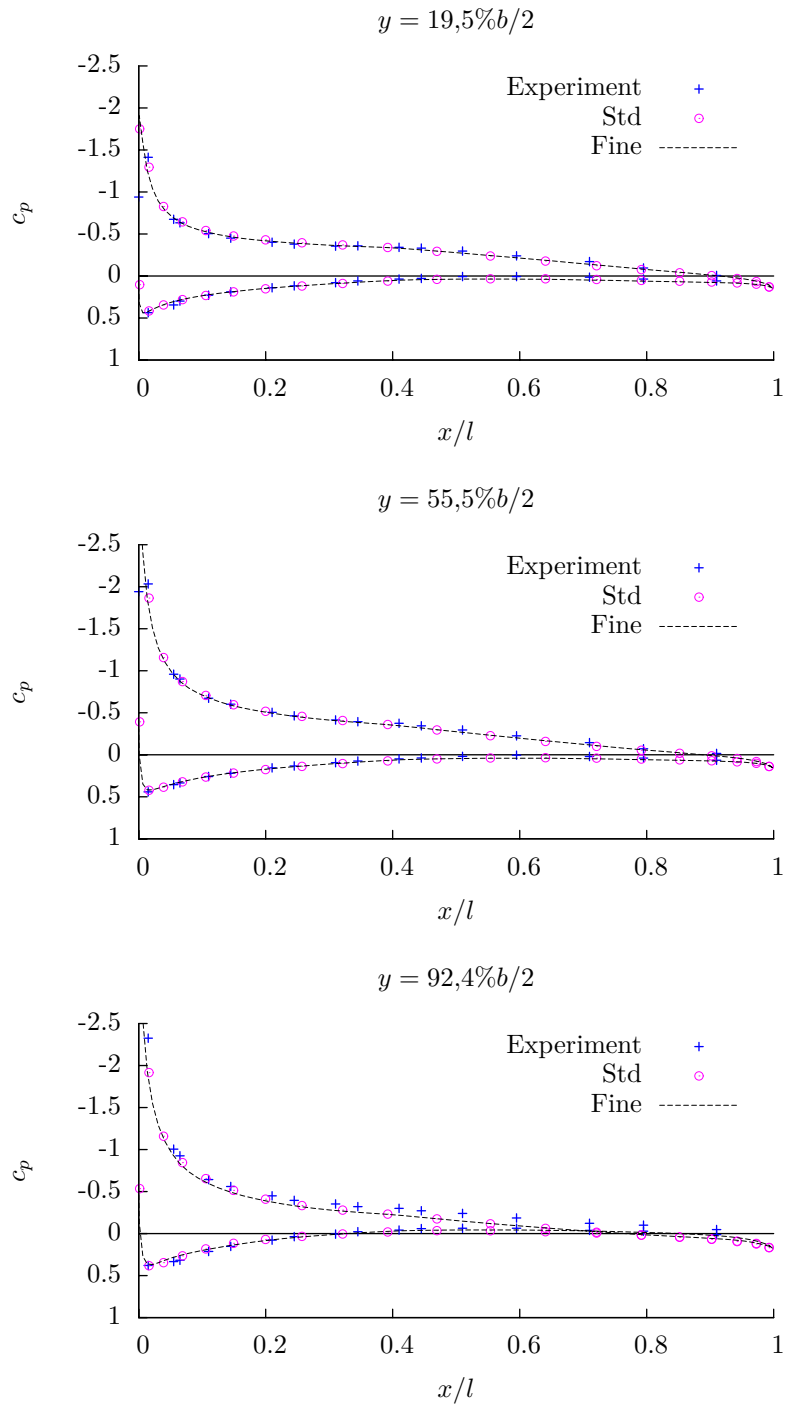


Figure 3.5: Comparison of the pressure distribution on the swept wing

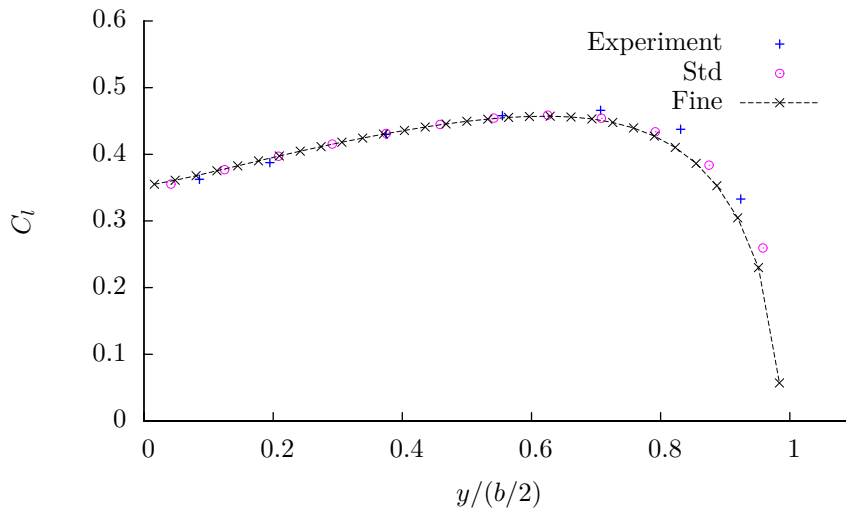


Figure 3.6: Comparison of the lift distribution on the swept wing

3.1.3 Boxwing

As a more complex configurations, a Boxwing will be investigated. CFD results are available from [3] where a series of generic boxwings with different dimensions was analysed. Figure 3.7 depicts the parametrization of the wing chord c , semi span $b/2$, radius R , and height h . Further, the coordinate η denotes the normalized spanwise position. The wing root is at $\eta = 0$ and the transition to the radius is at $\eta = 1$.

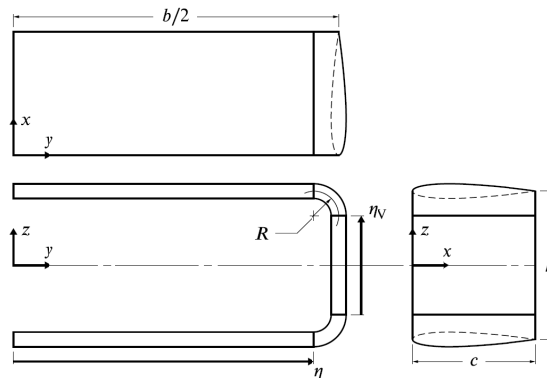


Figure 3.7: Definitions of the Boxwing [3]

For simplicity, this report is limited to a certain configuration within that series of different Boxwings. The selected configuration is the one for which the most data are available in [3]: $b = 12c$, $R = 0.15c$ and $h/b = 0.2$. The airfoil NACA0012 is constant over the entire perimeter and is not twisted. The CFD model consists of NURBS-Surfaces which allow a smooth radius in the transition between the horizontal and the vertical wings sections, respectively. In Aeolus ASP, this radius is being modeled by a finite number of support sections, as shown in Fig.3.8.

These support sections can easily be introduced by a stepwise change of the dihedral in Aeolus ASP, so that modelling effort is low. In the CFD analysis, the lift coefficient was chosen

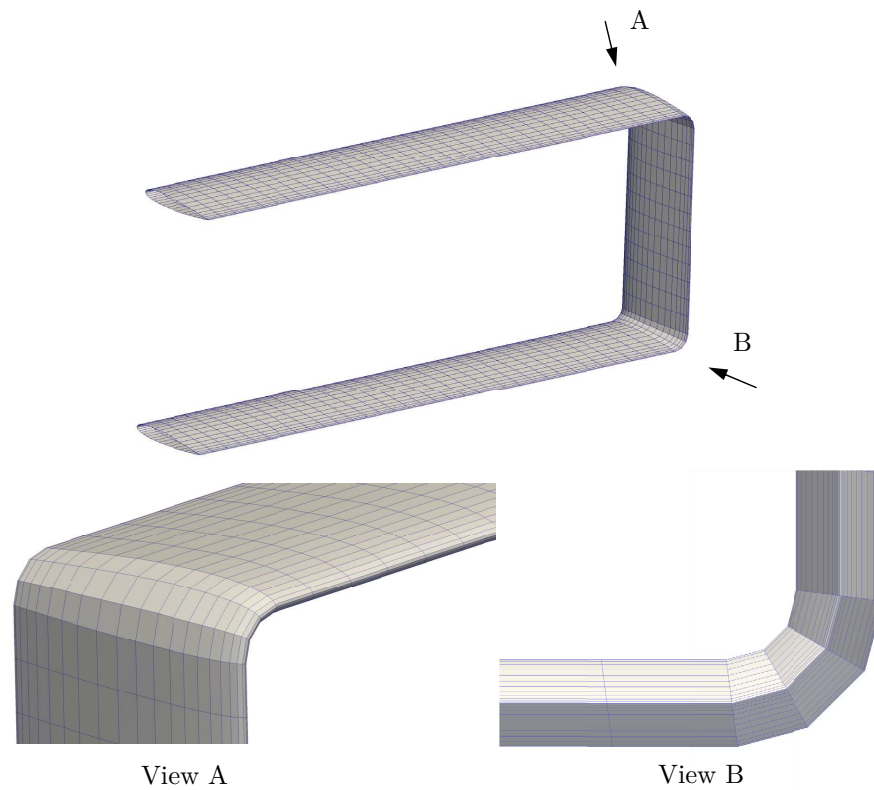


Figure 3.8: Support sections discretize the radius

to be $C_l = 0.5$. Under this condition, Aeolus ASP yields the pressure distribution shown in Fig.3.9, and the spanwise lift coefficient distribution shown in Fig.3.10 for both upper and lower horizontal wing.

The associated angle of attack α_∞ was determined to be 5.4058° in the CFD analysis and 5.572° in Aeolus ASP, which is a 3.1% difference.

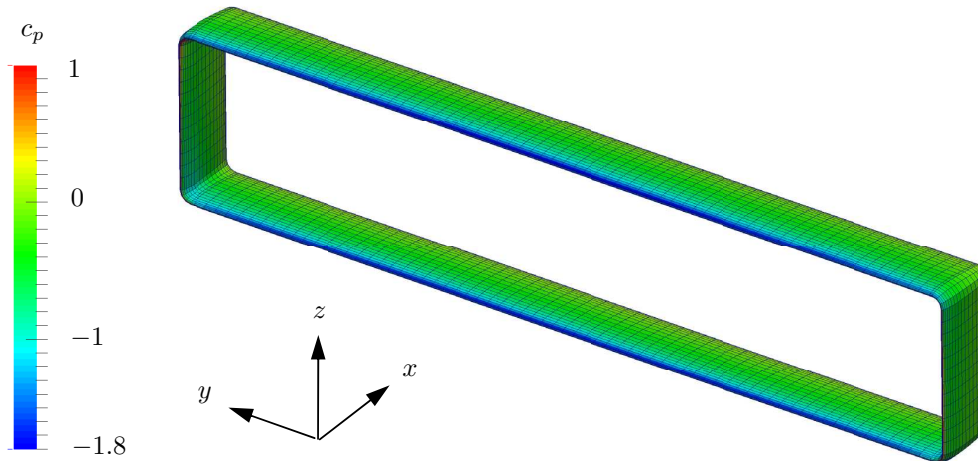


Figure 3.9: Aeolus ASP computed pressure distribution on the Boxwing (std resolution)

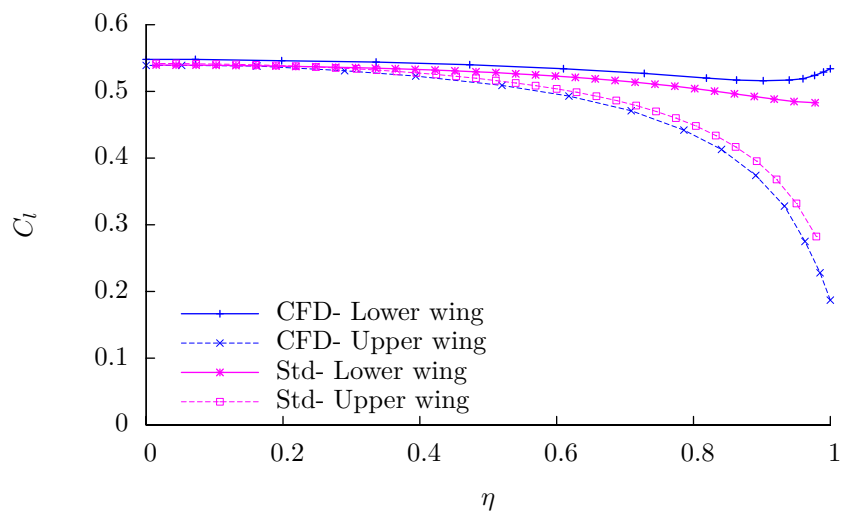


Figure 3.10: Comparison of the lift distribution for the Boxwing at $C_l = 0.5$

3.2 Induced drag

With regard to induced drag, the available and accessible experimental data are very limited. This is particularly true for unconventional wing configurations. Therefore, the validation of induced drag will be based on a comparison with CFD analysis and known solutions from lifting line theory, respectively.

3.2.1 Comparison with CFD

The above described Boxwing will be reused for this example. From [3, Fig.3b], a value of $e = 1.4388$ was determined for the non-twisted Boxwing, where e is the product of the Oswald factor and the span-efficiency factor. From the definition

$$e := \frac{F_l^2}{\pi b^2 F_{di}} \quad (1)$$

$$= \frac{S_{\text{ref}} C_l^2}{\pi b^2 C_{di}} \quad (2)$$

and the projected reference area $S_{\text{ref}} = 24c^2$, $b = 12c$, and $C_l = 0.5$ we find $C_{di} = 0.009218$ as the CFD reference value for the considered Boxwing. The value computed in Aeolus ASP is $C_{di} = 0.009069$, which corresponds to a -1.6% difference.

3.2.2 Robustness in an optimization

The objective of this section is to show, that the computation of induced drag is robust enough to be employed in wing shape optimization problems. Therefore, an optimization problem will be set up which aims optimize the wing twist such that the Lift/Drag-ratio reaches a maximum. The straight wing will be used as well as three additional swept Boxwings with different sweep angles, as shown in Table 3.1.

Table 3.1: Wing configurations

	b [m]	c [m]	ϕ [deg]	Airfoil
Straight wing	16	2,0	0	NACA0015
Boxwing 1	16	1,6	-30	NLF(1)-0115
Boxwing 2	16	1,6	0	NLF(1)-0115
Boxwing 3	16	1,6	+30	NLF(1)-0115

The Lift/Drag-ratio E depends on the lift distribution. The optimizer may change the lift distribution by changing the wing twist at certain spanwise stations. For the straight wing, Fig.3.11 shows six equidistant wing sections, which can be individually twisted by $\pm 10^\circ$. In a similar fashion, this is shown for the Boxwing in Fig.3.12 where nine sections may be twisted individually.

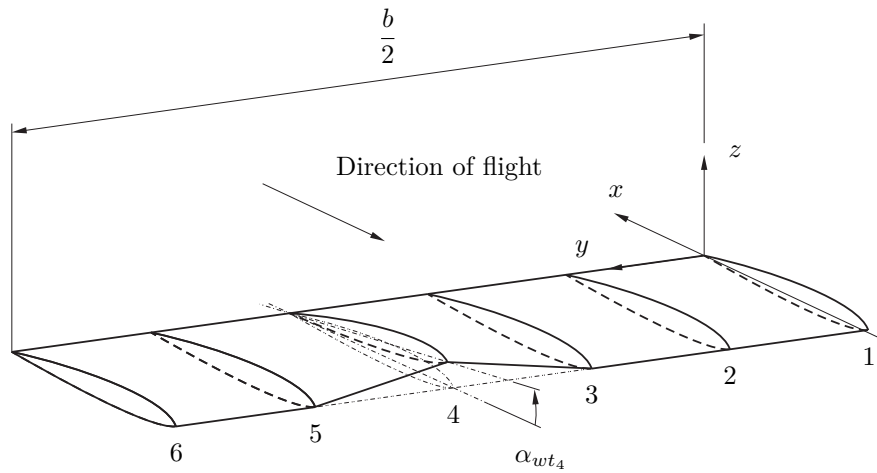


Figure 3.11: The straight wing has six twistable sections

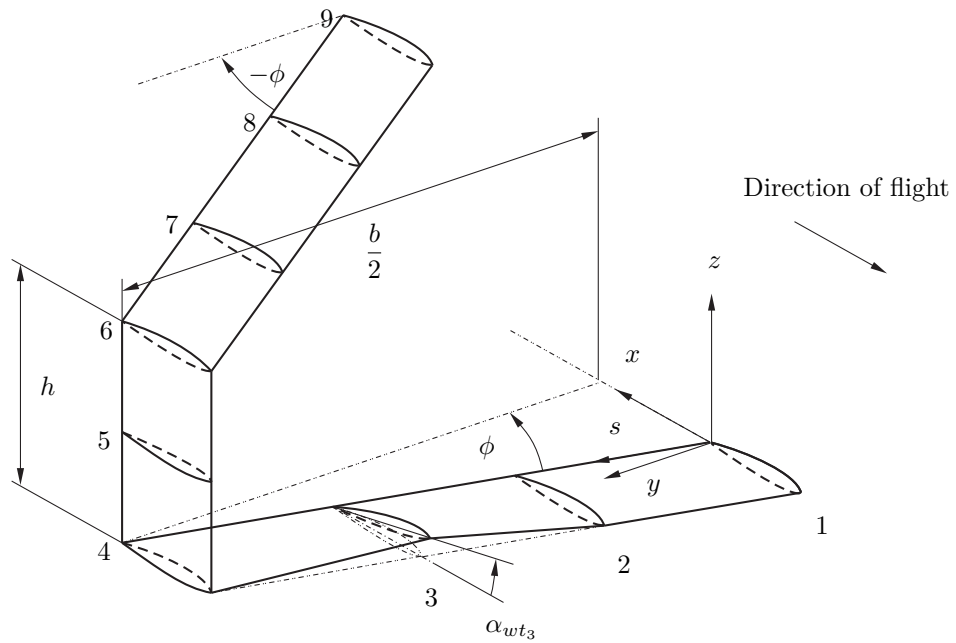


Figure 3.12: The Boxwing has nine twistable sections

Finally, the optimized Lift/Drag-ratio E can be compared to the theoretical value, which is known for these configurations from the following discussion. The Lift/Drag-ratio

$$E = \frac{C_l}{C_d} \quad (3)$$

contains the total drag coefficient

$$C_d = \frac{C_l^2}{\pi\Lambda e} + \beta C_{dvisc} \quad (4)$$

which is comprised of an induced and a viscous portion. For the present examples, the coefficient of viscous drag is $C_{dvisc} = 0.008$. The factor β accounts for the increased wetted surface of the Boxwing. This allows maintaining the projected wing surface as the coefficient's reference surface. The height-to-span-ratio of the Boxwing is $h/b = 0.2$ which yields $\beta = 1.2$ for the Boxwing, whereas $\beta = 1$ for the straight wing. The maximum E is

$$E_{max} = \left[2\sqrt{\frac{\beta C_{dvisc}}{\pi\Lambda e}} \right]^{-1} \quad (5)$$

When the wing is optimally twisted, the Oswald factor of the straight wing is $e = 1.0$, whereas a Boxwing with $h/b = 0.2$ may have a maximum $e = 1.464$ [4]. According to Munk's stagger theory, the induced drag remains constant when the Boxwing's upper and lower wing surface are translated in the streamwise direction. That is, the sweep angle has no effect on the maximum Lift/Drag-ratio as long as the stream-wise direction is parallel to the x-axis. In this study, however, there might be a small angle (depending on the twist distribution) but the impact is considered negligible. Table 3.2 summarizes the resulting values from Eq.(5). The Aeolus ASP results are shown in Table 3.3. Aeolus ASP does rather underestimate the wing performance.

Table 3.2: Maximum possible Lift/Drag-ratio of the considered configurations

	C_{dvisc}	β	e	$\Lambda = \frac{b^2}{S_{proj}}$	E_{max}
Straight wing	0.008	1.0	1.0	8.0	28.02
Boxwing 1	0.008	1.2	1.464	5.0	24.43
Boxwing 2	0.008	1.2	1.464	5.0	24.43
Boxwing 3	0.008	1.2	1.464	5.0	24.43

Table 3.3: Wing efficiency comparison

	Theory		Aeolus ASP		Difference	
	E^{max}	e	E^{max}	e	ε_E	ε_e
Straight wing	28.02	1.0	27.50	0.963	-1.86 %	-3.70 %
Boxwing 1	24.43	1.464	24.35	1.450	-0.33 %	-0.96 %
Boxwing 2	24.43	1.464	24.48	1.465	0.20 %	0.06 %
Boxwing 3	24.43	1.464	24.05	1.414	-1.56 %	-3.41 %

However, the relative difference of E and e is small. Finally, Fig.3.13 shows the optimized

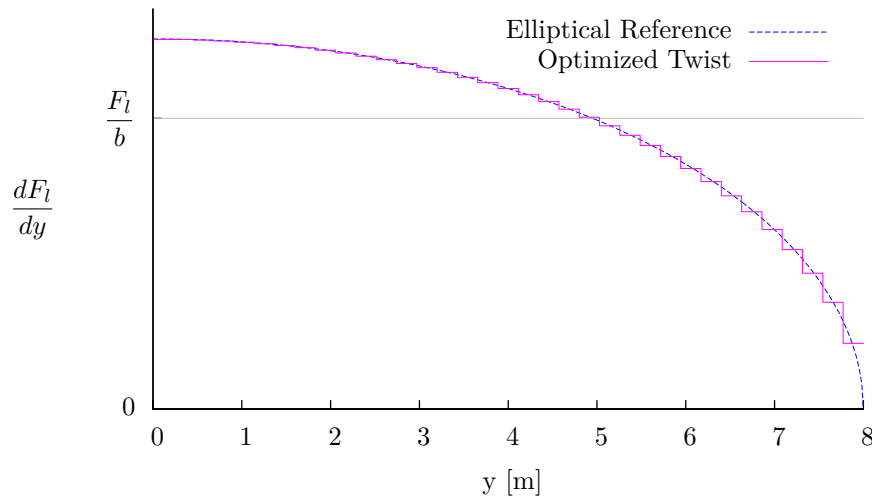


Figure 3.13: Lift distribution of the optimized straight wing

straight wing lift distribution as a step-wise function (over all wing strips) and the very good agreement to an optimal, elliptical distribution.

4 Conclusions

The good agreement of wind tunnel experiments, and CFD analyses with Aeolus ASP was demonstrated for a straight wing, a highly swept wing, and non-planar Boxwing configurations. It might be concluded that the proposed standard resolution is suitable for a wide variety of wing configurations. In particular, the difference between CFD and Aeolus ASP was found to be in the order of 1-4% for lift, drag, and AOA, respectively. Also, the induced drag analysis is robust enough to be applied in wing shape optimization problems.

References

- [1] MCALISTER, K. W. ; TAKAHASHI, R. K.: NACA 0015 Wing Pressure And Trailing Vortex Measurements. In: *NASA-TP-3151* (1991)
- [2] KOLBE, Carl D. ; BOLTZ, Frederick W.: *The Forces and Pressure Distributions at Subsonic Speeds on a Plane Wing Having 45 degrees of Sweepback, Aspect Ratio of 3, and a Taper Ratio of 0.2*. NACA-RM-A51G31, 1951
- [3] GAGNON, Hugo ; ZINGG, David W.: Aerodynamic Optimization Trade Study of a Box-Wing Aircraft Configuration. In: *Journal of Aircraft* 53 (2016), 2016/03/14, Nr. 4, S. 971 – 981. ISBN 0021-8669
- [4] KROO, Ilan M.: Nonplanar Wing Concepts for Increased Aircraft Efficiency. In: *VKI lecture series on Innovative Configurations and Advanced Concepts for Future Civil Aircraft* (2005)

List of Figures

2.1	Overview of investigated wing configurations	3
3.1	Aeolus ASP computed pressure distribution on the straight wing (std resolution)	5
3.2	Comparison of the pressure distribution on the straight wing	6
3.3	Comparison of the lift distribution on the straight wing	7
3.4	Aeolus ASP computed pressure distribution on the swept wing (std resolution) .	7
3.5	Comparison of the pressure distribution on the swept wing	8
3.6	Comparison of the lift distribution on the swept wing	9
3.7	Definitions of the Boxwing	9
3.8	Support sections discretize the radius	10
3.9	Aeolus ASP computed pressure distribution on the Boxwing (std resolution) . . .	11
3.10	Comparison of the lift distribution for the Boxwing at $C_l = 0.5$	11
3.11	The straight wing has six twistable sections	13
3.12	The Boxwing has nine twistable sections	13
3.13	Lift distribution of the optimized straight wing	15

List of Tables

2.1	Overview of wing parameters and available reference results	4
2.2	Investigated panel resolutions in Aeolus ASP	4
3.1	Wing configurations	12
3.2	Maximum possible Lift/Drag-ratio of the considered configurations	14
3.3	Wing efficiency comparison	14